ACS APPLIED NANO MATERIALS

www.acsanm.org Article

Layer-By-Layer Polyelectrolyte Assembly for the Protection of GaP Surfaces from Photocorrosion

Nikolay V. Ryzhkov, Olesya Ledovich, Lara Eggert, Andreas Bund, Agnieszka Paszuk, Thomas Hannappel, Konstantin Klyukin, Vitaly Alexandrov, and Ekaterina V. Skorb*

Cite This: *ACS Appl. Nano Mater.* 2021, 4, 425−431 Read Online

ACCESS | Metrics & More | Article Recommendations

ABSTRACT: Polyelectrolyte layer-by-layer assemblies are known as protective coatings for corrosion inhibition. Here, we demonstrate that polyelectrolyte multilayers of poly(ethyleneimine) (PEI) and poly(styrene sulfonate) (PSS)—$(PEI/PSS)_x$—adsorbed at the GaP(100) photocathode surface remarkably mitigate the photocorrosion of GaP without decreasing its photoconversion efficiency. The activity of the polybase−polyacid complex is based on buffering pH changes at the solid−liquid interface. We carried out ab initio molecular dynamics-based simulations of the GaP(100) surface in contact with liquid water and demonstrated that an increase in the proton concentration enhances GaP dissolution. We used the scanning vibrating electrode technique (SVET) to characterize the distribution of photocorrosion activity areas over bare and polyelectrolyte-coated GaP surfaces and we showed that a polyelectrolyte coating impedes the dissolution kinetics. Data obtained using the SVET were compared to photoetched pores on the semiconductor surface. Voltammetric and chronoamperometric measurements were also performed to evaluate photoconversion efficiencies before and after the application of the protective coatings.

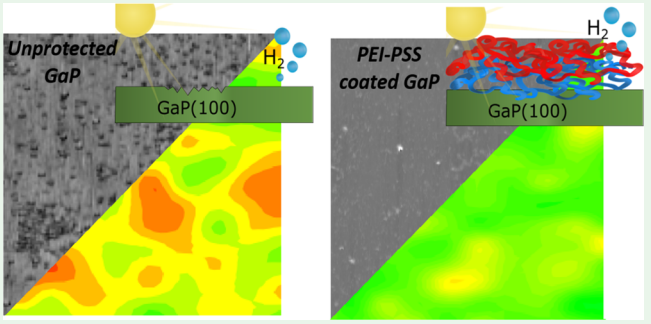

KEYWORDS: *polyelectrolytes, layer-by-layer assembly, proton sponge, III−V semiconductors, photocorrosion*

INTRODUCTION

Energy conversion using solar irradiation is a perspective and sustainable way to obtain clean and renewable fuels.[1] World-record conversion efficiencies in both photovoltaics[2] and solar water splitting[3] are achieved with multijunction solar cells based on III-V compound semiconductor structures. Despite the outstanding efficiency of hydrogen production under solar light irradiation,[4] the widespread use of these materials is limited by their oxidative corrosion.[5,6]

A promising photocathode for solar-to-hydrogen conversion is GaP, as its band gap is well-aligned to the water reduction accompanied by hydrogen production.[7] However, emerging holes can trigger the anodic dissolution of the material (Figure 1a) according to eq 1 in acidic solutions[8]

$$GaP + 3H_2O + 6h^+ = Ga^{3+} + 3H^+ + H_3PO_3 \quad (1)$$

and according to eq 2 in alkali ones[8]

$$GaP + 4OH^- + 3h^+ = GaO_2^- + P + 2H_2O \quad (2)$$

Indeed, photocathodes made of GaP are reported to be unstable and the rate of photodegradation depends significantly on the electrolyte's nature.[6] Previous observations indicated that GaP is quite unstable under both acidic and basic conditions, whereas GaP photocorrosion is significantly suppressed at neutral pH.[9] It is obvious that the photoelectrochemical decomposition of water on the photoelectrode leads to pH changes at the interface. Thus, high-value III−V semiconductor materials require pH buffering at the semiconductor/solution interface for improved performance and durability.

Based on this, a very effective solution for the deposition of protective coatings is the layer-by-layer (LbL) procedure, which involves the stepwise electrostatic assembly of oppositely charged polymer molecules and allows the formation of coatings with multiple functionalities.[10,11] LbL-assembled polyelectrolyte coatings have been proven to efficiently protect metals from corrosion.[12,13] The phenomenon of their anticorrosion performance can be explained by three mechanisms: (i) weak polyelectrolytes exhibit a pH-buffering activity and can stabilize the pH level;[14,15] (ii) protons occurring at the solid−liquid interface and assisting

Received: October 16, 2020
Accepted: December 17, 2020
Published: December 31, 2020

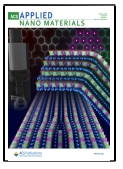

https://dx.doi.org/10.1021/acsanm.0c02768
ACS Appl. Nano Mater. 2021, 4, 425−431

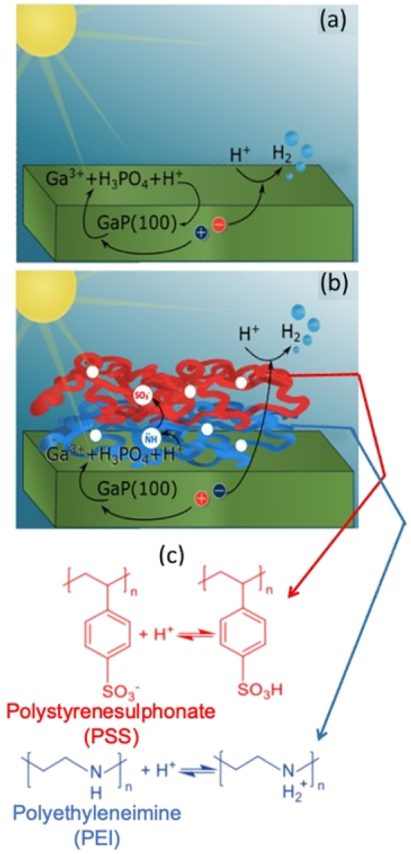

Figure 1. Schematic representation of photoinitiated processes at the (a) GaP−water solution interface: light-induced charge separation occurs in GaP; the electrons captured by protons in the water solution lead to hydrogen evolution and holes lead to anodic dissolution of GaP and local acidification of corrosive area, promoting further corrosion. As a result, under illumination, the photoelectrode surface is etched and the photocurrent and the photoconversion efficiency decrease; (b) PEI/PSS-protected GaP(100) surface: protons produced during GaP anodic dissolution are captured by PEI, proton "sponge" weak polyelectrolyte, and then PSS, strong polyelectrolyte; as a result, pH-buffering at the GaP/water solution interface inhibits semiconductor anodic dissolution, surface etching occurs to a lesser extent, and the photocurrent is stabilized.

corrosion can be captured by polyelectrolyte molecules,[16] and (iii) the polyelectrolytes that form the coating are relatively mobile[17] and have the tendency to seal and eliminate mechanical cracks of the coating, performing self-healing. All the mechanisms mentioned above could also be useful for III−V semiconductor photocorrosion protection. Furthermore, nanometer-thick polyelectrolyte multilayers are optically transparent[18] and permeable for water and smaller ions,[19] which is important in solar water-splitting applications. Recent studies also showed that polyelectrolyte layer formation on top of photoelectrodes of various natures does not lead to impedance growth.[20,21] In this paper, we studied the stability of bare and polyelectrolyte-coated p-type GaP(100) during operation under solar light. Hereby, in this paper, we focus on the control of the photochemical response of the hybrid system based on GaP, which can significantly change its long-term performance in the aqueous solution.

A smart multilayered system consisting of a strong−weak polyelectrolyte assembly deposited on GaP(100) substrates providing pH buffering at the semiconductor−solution interface is observed to prevent photocorrosion of the photoelectrode material. We also present the calculations that justify our strategy for protecting the material against corrosion by its interface pH-buffering. Anodic dissolution of GaP under illumination in solution is characterized in situ. Also, the effects of photocorrosion on material morphology and performance are shown.

RESULTS AND DISCUSSION

GaP Dissolution Mechanism and pH-Buffering Strategy to Inhibit GaP Photocorrosion. When cathodic hydrogen production and the anodic process described in (1) occur simultaneously, they can be combined to obtain the overall scheme of the corrosion process at the GaP−water solution interface when this is irradiated

$$GaP + 3H_2O + 3H^+ = Ga^{3+} + H_3PO_3 + 3H_2 \qquad (3)$$

Equation 3 shows that protons are converted to hydrogen and drive the process of photoelectrode dissolution.

To demonstrate the critical role that an acidic environment may play in facilitating the dissolution of GaP, we have also

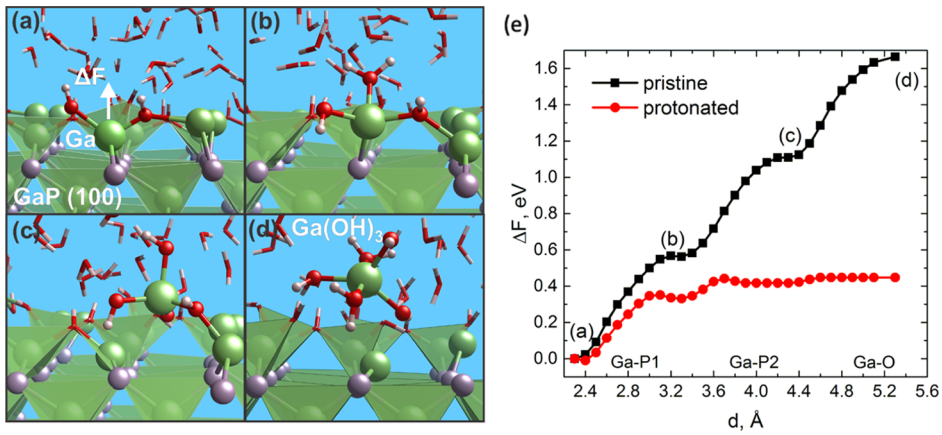

Figure 2. (a−d) Scheme showing the identified mechanism of Ga dissolution from the GaP (100) surface in an aqueous solution (color scheme: Ga—green, P—gray, O—red, and H—white): (a) Ga−P bond breaking, (b) Ga−H_2O bond formation, (c) second Ga−P bond breaking and Ga release to the surface, (d) Ga−O bond breaking and desorption of a $Ga(OH)_3$ complex; (e) corresponding free-energy profiles for the pristine and protonated GaP (100) surfaces in contact with water. The graph is composed of three parts corresponding to breaking the two Ga−P and single Ga−O bonds chosen as collective variables in each interval.

https://dx.doi.org/10.1021/acsanm.0c02768
ACS Appl. Nano Mater. 2021, 4, 425−431

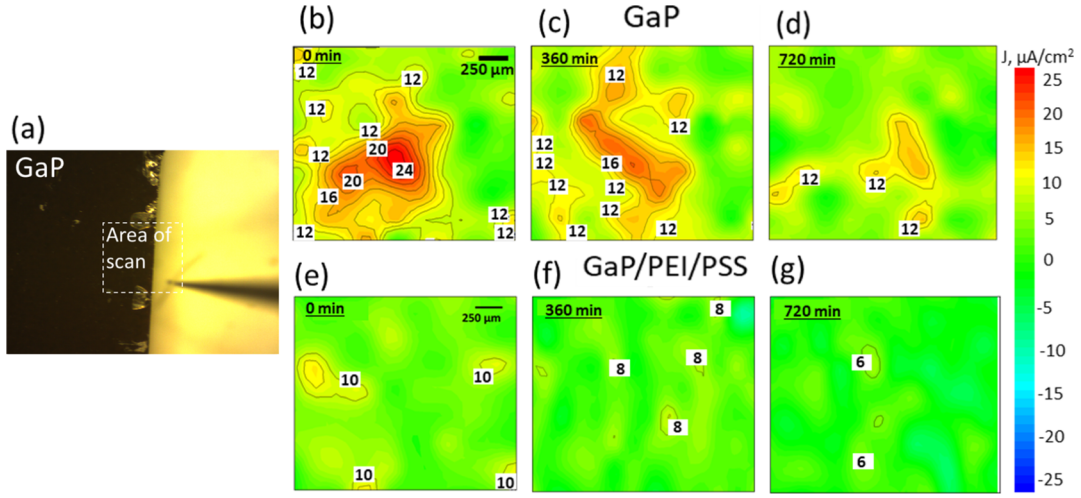

Figure 3. (a) Optical image of the GaP photoelectrode scanned using an SVET probe. The scanned area at the edge of the GaP specimen is shown by the white dotted frame, (b–d) series of long-term SVET scans over the pristine GaP surface at an open circuit obtained after (b) 1–15 min of illumination, (c) 360–375 min of illumination, and (d) 705–720 min of illumination, (e–g) series of long-term SVET scans over the GaP/PEI/PSS surface at an open circuit obtained after (e) 1–15 min of illumination, (f) 360–375 min of illumination, and (g) 705–720 min of illumination, SVET scans were registered in 0.05 M NaCl solution.

undertaken ab initio molecular dynamics (AIMD)-based simulations of the GaP (100) surface in contact with liquid water. Previous AIMD calculations of the pristine GaP and InP (100) surfaces[23,24] exposed to water have identified surface hydroxylation motifs and revealed distinct hydrogen-bond strength and proton-transfer dynamics at the two semiconductor/water interfaces. Our AIMD simulations started with a fully equilibrated Ga-rich GaP (100)/water interface where we observed a combination of free and bridging chemisorbed hydroxyl groups and molecular water. These surface groups are found to be in dynamic equilibrium because of the facile local proton transfer, in full agreement with prior AIMD simulations.[23,24] To demonstrate an effect of surface protonation on GaP dissolution kinetics, we examined the dissolution of Ga from a representative interfacial configuration, as shown in Figure 2. Here, Ga is coordinated by one bridging OH, one free OH, and two subsurface P atoms. To estimate activation barriers of Ga dissolution, we applied a slow-growth approach in combination with the thermodynamic integration technique as implemented in VASP (see the Computational Methodology section).

We first modeled Ga dissolution under pH-neutral conditions and found that Ga dissolution starts with the subsequent breaking of the two Ga–P bonds. After the first bond is broken (Figure 2a), Ga forms a new bond with the nearest H_2O molecule resulting in a metastable state (Figure 2b) with a very flat minimum characterized by an activation barrier of 0.61 eV. Then, the system overcomes a barrier of 0.51 eV, which involves the breaking of the second Ga–P bond, dissociation of H_2O, and release of Ga to the surface (Figure 2c). The last dissolution step is the desorption of $Ga(OH)_3$ from the surface into solution by breaking the remaining Ga–O bond. This step takes about 0.56 eV to break a single Ga–O bond (Figure 2c,d). Figure 2e (black line) shows a free energy profile for the pristine GaP (100) surface in contact with water.

To evaluate the impact of local pH changes on Ga dissolution rates, we then introduced additional protons to the system. These protons can diffuse into the semiconductor interior and protonate subsurface P atoms adjacent to the dissolving Ga atoms disrupting the Ga–P bond topology. Herein, we did not examine the mechanism and kinetics of proton diffusion through the surface; however, this process was demonstrated for other semiconductor materials.[25] Moreover, proton transfer into the subsurface will be facilitated after the dissolution process has started and in the presence of surface irregularities. As seen in Figure 2e (red line), protonation of P atoms weakens the structural Ga–P bonds leading to more stable intermediate states and considerably lower activation barriers. It is found that after a subsequent protonation of adjacent P atoms, the cumulative dissolution barrier drops down to 0.48 eV, which should result in dissolution kinetics that are several orders of magnitude enhanced relative to pH-neutral conditions.

The magnitude of the effect at medium pH values is seen from our AIMD-based simulations of dissolution barriers discussed above. The predicted difference in interfacial behavior may be achieved by the pH-buffering performance of polyelectrolyte layers on the semiconductor surface.

We thus conclude that the strategy to prevent GaP photocorrosion is pH stabilization at the semiconductor–liquid interface. This could be achieved by the formation of a coating with a pronounced pH-buffering activity on the semiconductor surface. Nanometer-thick[26] LbL-assembled coatings are good candidates.[15] They do not prevent charge transfer at the solid–liquid interface maintaining photoconversion efficiency[20,21] but inhibit direct interaction of GaP with protons in solution, impeding corrosion. Branched cationic polyethyleneimine (PEI) was used as a first layer. This polymer is a weak polybase exhibiting buffering properties because the closely spaced amino groups are able to take up H^+ ions from the solution.[27] Because PEI has a limited buffer capacity, its single layer on the GaP photoelectrode surface will not give the desired long-term effect. Therefore, poly(sodium-4-sterenesulphonate) (PSS) was deposited on top of the GaP/PEI. PSS is a strong polyanion and cation-exchange polymer which, in combination with PEI, allows better pH-buffering the semiconductor/solution interface. Our strategy to prevent GaP photocorrosion by depositing buffering multilayers combining

https://dx.doi.org/10.1021/acsanm.0c02768
ACS Appl. Nano Mater. 2021, 4, 425–431

proton "sponge" and proton conductive layers is demonstrated in Figure 1b.

GaP Photocathode Corrosion Inhibition. With proton consumption from solution and their conversion to H_2, pH of the near-electrode region is expected to shift to basic values.[22] Because acidic electrolytes (e.g., 1 M H_2SO_4) are usually utilized to produce hydrogen, it is unlikely that a strongly alkaline medium is formed at the interface. Therefore, further we focused on corrosion processes in acidic electrolytes. In this case, protons in solution can serve not only as acceptors of photoelectrons but also interact with the material of the photoelectrode, contributing to its photocorrosion.

Furthermore, according to eq 1, gallium phosphide photoanodic dissolution is accompanied by acidification at the photoelectrode−solution interface in areas where corrosion process is localized. As will be shown later (Figures 3 and 4), corrosion does not occur on the entire surface of the illuminated photoelectrode but only in some regions (e.g., where crystal defects are localized). Therefore, even in neutral electrolytes, a local shift of pH toward lower values can occur in places where corrosion processes are localized. These locally formed protons can influence corrosion processes before being converted to hydrogen.

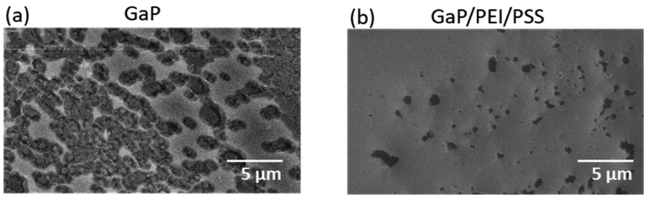

Figure 4. SEM images of the photoelectrode surface for (a) pristine GaP after 12 h of illumination in 1 M KCl, (b) GaP/PEI/PSS after illumination under mild conditions of 1 M KCl.

To demonstrate the validity of the model considered in the previous chapter and the protective performance of the proposed polyelectrolyte coating of $(PEI/PSS)_x$ architecture, we performed an SVET analysis of pristine- and polyelectrolyte-protected photoelectrode surfaces under illumination in the electrolyte solution. This technique allows us to visualize the distribution of anodic and cathodic activity regions by measuring the electric field in a solution near the sample surface. The measurements by SVET were carried out under open-circuit conditions. The reason is an external electric field arising in the solution upon polarization of the photoelectrode. It might be so high that the electric fields arising during corrosion could not be recorded using an SVET device.

The uniformly illuminated (visible irradiation, 11,000 lumen) area at the edge of the planar GaP specimen was studied by SVET in 0.05 M NaCl solution at pH ∼7. The scanned area included both the space above the photoactive sample and the spaces above the region without the sample; thus, the test and control samples were studied simultaneously under the same conditions during a single experiment (Figure 3a).

Over a pristine GaP sample, anodic activity spots were observed. The interfacial reactions occurring at open-circuit potential can be attributed to the anodic dissolution of the photoelectrode material coupled with photocathodic proton reduction according to the scheme from Figure 1a. It is worth noting that despite the uniform illumination, the areas of anode activity are localized only in some parts of the sample (Figure 3b). This supports the assumption that the observed anode activity is related to the dissolution of the photoelectrode because of its photocorrosion. Lattice defects introduce energy states within the valence band which are more likely to be populated with the photoexcited holes. Therefore, photocorrosion initially starts and evolves at lattice defects. This determines the pattern of the anodic activity observed on the SVET scan. The sample was scanned continuously for 12 h, allowing us to observe the evolution of the GaP photoanodic dissolution (Figure 3b−d).

Photocorrosion is observed during the early times of illumination. We suppose that it occurs under open-circuit conditions because there is no way of holes outflow but photoelectrode material self-oxidation. Also, we can conclude that anodic dissolution fades over time possibly because of the surface passivation, accompanying the photocorrosion of the GaP under neutral-pH conditions.[9]

When the GaP photoelectrode surface is coated by a polyelectrolyte multilayer of PEI/PSS, anodic dissolution is suppressed according to SVET scanning. Absolute values of the anodic activity in terms of ionic current are 2.5 times lower and the anodic activity localization area is more than 10 times smaller (Figure 3e−g). Photocorrosion processes usually develop fast after disruption of the surface atomic order. However, polyelectrolyte coatings being adaptive and dynamic materials respond to local changes in pH and ionic strength by polymer network reorganization.[28] Apparently, coating self-healing occurs[29] and stable low anodic activity is observed over polyelectrolyte-coated GaP.

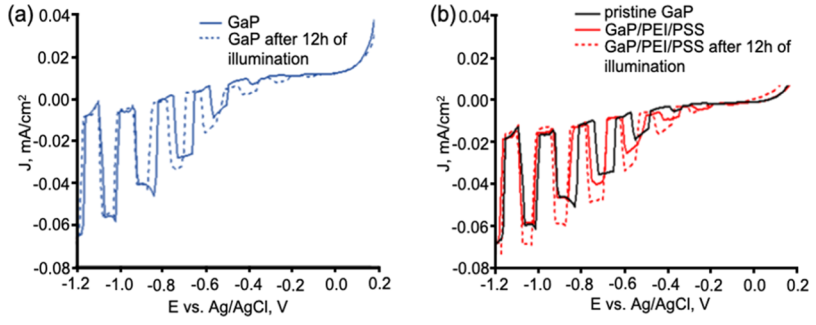

Figure 5. (a) Current−potential curves under chopped illumination of pristine GaP(100), black line—previously unused GaP specimen and black dotted line—the same specimen after 12 h of operation under illumination (11,000 lumen) in 1 M KCl solution; (b) current−potential curves under chopped illumination of: black line—previously unused pristine GaP, red line—the same specimen of GaP after PEI/PSS deposition, and red dotted line—GaP/PEI/PSS after 12 h of operation under illumination (11,000 lumen) in 1 M KCl solution.

https://dx.doi.org/10.1021/acsanm.0c02768
ACS Appl. Nano Mater. 2021, 4, 425−431

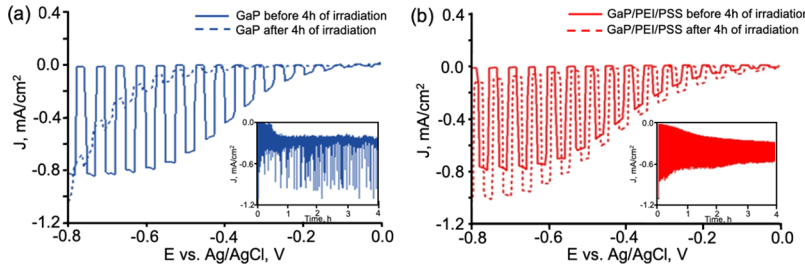

Figure 6. Current−potential curves registered in 1 M H_2SO_4 solution under chopped illumination (11,000 lumen) of (a) pristine GaP, black line—before irradiation and black dotted line—the same specimen after 4 h illumination at −0.6 V vs Ag/AgCl; (b) GaP/PEI/PSS red line—before irradiation and red dotted line—the same specimen after 4 h illumination at −0.6 V vs Ag/AgCl; insets are chronopotentiometry curves during 4 h under chopped illumination at −0.6 V vs Ag/AgCl.

The effects of photocorrosion on the morphology of the photoelectrode at the microscopic level were studied by SEM. Figure 4a demonstrates the surface of the GaP photoelectrode after 12 h of illumination under neutral conditions. Although the initial GaP surface was smooth and relatively featureless, the formation of pores was observed after operation under illumination in agreement with maps of photoanodic activity registered using the SVET (Figure 3b−d). Despite the passivation of the surface over time, significant surface defects are formed. After depositing a protective layer, anodic dissolution is suppressed according to SVET data (Figure 3e−g) and the photoelectrode surface is etched in a lower degree (Figure 4b).

Thus, the deposition of a buffering polyelectrolyte multilayer allows us to suppress the anodic dissolution of GaP, and nanometer-thick polyelectrolyte PEI/PSS coating provides effective photocorrosion inhibition.

Photocurrent Degradation Prevention. The effect of polyelectrolyte layers on the photoactivity of GaP photocathodes was studied under chopped visible irradiation (11,000 lumen) in a three-electrode cell in 1 M KCl. Figure 5 demonstrates typical I−V plots. Cathodic photocurrent steadily increases with the potential becoming more negative whether polyelectrolytes are deposited on top of the surface or not. Polyelectrolyte layers neither affect the absorption of light by a semiconductor nor have a significant photosensitizing effect and almost the same profile of voltammetry curves was observed for bare (Figure 5a) and polyelectrolyte-coated GaP (Figure 5b). Furthermore, we observed that for the polyelectrolyte-coated GaP photoelectrode, a slight increase in the photocurrent values was observed. We suppose that it is due to surface area increase after rough polyelectrolyte coating formation.[21] For both bare and PEI/PSS-coated photoelectrodes, no photocurrent degradation during long-term operation under constant illumination (11,000 lumen) and −0.6 V versus Ag/AgCl polarization was observed. Thus, in the photo-electrochemical cell, in the mild ambience photocathode surface, etching does not lead to a decrease in the photoconversion efficiency and photocurrent degradation.

However, at neutral pH, photocurrent density values are rather small compared to recent reports for acidic solutions where proton conversion is the most effective.[4] Furthermore, we studied the ability of buffering polyelectrolyte layers to protect GaP from photocorrosion under acidic conditions (1 M H_2SO_4). Here, photocurrents increased by an order of magnitude because of the higher efficiency of proton-to-hydrogen conversion and a lower nonradiative recombination rate of photoexcited charge carriers. Nonetheless, under such conditions, the anodic dissolution of the photocathode leads rather quickly to photocurrent degradation. Figure 6a demonstrates the photocurrent decrease after photoelectrode operation at −0.6 V versus Ag/AgCl under illumination by visible light with 11,000 lumen intensity for 4 h, evidencing its significant photodegradation and the decrease in photoconversion efficiency in comparison with neutral conditions (Figure 5a). The photocurrent density is lower for pristine GaP photoelectrodes after long-time irradiation (Figure 6a), whereas for PEI/PSS-protected photocathodes, the effect of photocurrent decrease after operation under illumination is not so pronounced (Figure 6b).

Such a difference in the behavior of the photoelectrode in different electrolytes is in agreement with previously proposed mechanisms of GaP photocorrosion.[30] It was previously reported that during GaP anodic dissolution, Ga is going into solution in the form of hydroxide.[6] Meanwhile, this compound is not soluble in solutions of medium pH.[9,30] Thus, anodic oxidation of GaP under neutral conditions leads to the formation of a $Ga(OH)_3$ passivating layer, preventing further dissolution.[8] We suppose that it is a reason why we observed photoanodic activity decay on SVET scans (Figure 3b−d) and no significant photocurrent degradation in KCl solution of neutral pH for the bare GaP sample (Figure 5a). However, the passivation layer can be dissolved by acids and fresh electrode surface proceeds to corrode under illumination resulting in significant photocurrent degradation (Figure 6a).

With the time of irradiation for both samples (coated and uncoated with polyelectrolytes), an increase in the dark cathodic current was observed (Figure 6 a,b insets). For bare GaP, the growth of the dark current is observed mainly during the first hour, while for the sample coated with polyelectrolytes, this process is more extended in time and an increase in the dark current is observed for 1.5−2 h before stabilization. It should be noted that this is not a unique process; such changes have previously been shown in photoelectrodes based on Cr_2O_3,[31] for example. We suppose that this phenomenon could be explained by electrons leaking to defect and surface states emerging during photocorrosion of GaP.

Thereby, buffering with polyelectrolyte layers does not only prevent GaP dissolution in neutral media under illumination but also preclude its photodegradation and photoconversion efficiency decrease in strongly acidic media.

■ CONCLUSIONS

We have demonstrated an efficient strategy of soft matter assemblies for photocorrosion protection, particularly addressing III−V semiconductor systems. The smart coating

https://dx.doi.org/10.1021/acsanm.0c02768
ACS Appl. Nano Mater. 2021, 4, 425−431

assembled from weak proton "sponge" polycation PEI and strong polyanionic cationite PSS prevents anodic etching of p-type Zn-doped GaP photocathodes and enables its prolonged photoactivity. The mechanism of polyelectrolyte multilayer protective action is based on the pH-buffering capacity of a polyelectrolyte multilayer. The effect has been demonstrated on a surface relevant for water splitting devices, but it is expected to be applicable to many types of interfacial processes where pH-buffering is important.

MATERIALS AND METHODS

Chemicals and Materials. Poly(ethyleneimine) (PEI, $M_w \sim 70$ kDa) and poly(styrene sulfonate) (PSS, $M_w \sim 500$ kDa) were obtained from Sigma-Aldrich. Reagent-grade NaCl (99.5%) was obtained from Merck. All chemicals were used without further purification. p-type GaP (100) wafers with ±0.5° offcut Zn-doped to 1.8 to 2.3 × 10^{18} cm^{-3} were obtained from the Institute of Electronic Materials Technology (Warsaw, Poland).

Computational Methodology. Simulations were performed employing a 10.90 × 10.90 × 21.35 $Å^3$ box comprising the GaP slab and a vacuum gap of ∼10 Å. The surface was hydroxylated in accordance with previous studies[23,24] and the vacuum gap was filled with 34 H_2O to obtain a water density of ∼1 g/cm^3. To evaluate dissolution barriers, we applied Born-Oppenheimer molecular dynamics (BOMD) simulations in combination with slow-growth and Blue Moon ensemble techniques[32] within the plane-wave density-functional-theory formalism as implemented in the VASP code.[33] All simulations were performed employing the Perdew−Burke−Ernzerhof (PBE)[34] functional along with the projector-augmented wave (PAW) formalism and DFT-D3 van der Waals correction.[35] A 1.0 fs time step in the BOMD simulations and the hydrogen mass of 3 a.m.u. were used. To keep the charge neutrality of the simulation cell with additional protons into aqueous solution, we removed one/two protons from the absorbed water on the opposite side of the GaP slab. The Nose−Hoover thermostat was used to keep the simulation temperature around 300 K.[36] The trajectories obtained using the slow-growth approach as the energetically favorable reaction pathways were used for subsequent Blue Moon ensemble-based thermodynamic integrations to estimate activation barriers. A set of windows along each reaction pathway was chosen with a step of 0.1 Å between adjacent windows. Configurations in each window were additionally equilibrated during 2 ps, while the next 2 ps were used to collect and average the energy gradients along the reaction direction. A similar computational scheme was employed in a series of recent studies.[37−39]

Polyelectrolyte Multilayer Assembly. A single p-GaP (100) wafer was cut into several parts. Polyelectrolyte layers were deposited on top of GaP using the classical Lbl technique. The procedure of multilayer assembly consists in depositing alternating layers of oppositely charged materials with wash steps in between. In our case, it was accomplished by alternating immersion of the GaP specimen in a polyelectrolyte (PEI and PSS) in ambient light. Semiconductor plates were immersed in 2 mg/mL polyelectrolyte solution in 0.5 M NaCl for 15 min in ambient light. After the deposition of each layer, the specimen was rinsed with water and dried in air steam. To obtain more dense PEI coverage, the GaP plate was twice immersed in PEI solution before PSS deposition. Eventually, PEI/PSS coating was obtained on top of the GaP substrate.

Local Photo-electrochemical Study. Photoactivity of pristine- and polyelectrolyte-covered, p-type, Zn-doped GaP(100) was studied under irradiation using the SVET. This method allows the observation of the material's electrochemical activity with micrometer spatial resolution and outstanding sensitivity. The potential, ΔV, between two points at a distance Δr from each other was measured for these purposes. It is realized using a vibrating (with amplitude Δr) probe scanning the surface of the irradiated specimen. To perform the SVET study, a system from Applicable Electronics (USA) under control of ASET program (Sciencewares, USA) was used. Pristine- or polyelectrolyte-covered GaP(100) samples under investigation were attached to an epoxy holder using adhesive tape. The surface of the photoelectrode was uniformly illuminated by visible light (luminous power 11,000 lumen) and scanned using the vibrating probe. The scanning area was selected on the edge of the specimen. As a vibrating probe for the SVET experiments, insulated Pt−Ir microprobes (Microprobe Inc., USA) with a platinum black spherical tip of 30 μm diameter were applied. The probe was vibrating in two directions parallel and perpendicular to the specimen surface 150 μm above it. The amplitude of vibration was 30 μm, and vibration frequencies of the probe were 136 Hz (perpendicular to the surface) and 222 Hz (parallel to the surface). Data were presented in terms of ionic currents. The ionic current density was mapped on a 40 × 40 grid in a 0.05 M NaCl solution. The time of acquisition for each SVET data point was 0.6 s.

Photocurrent Measurements. Photo-electrochemical measurements were performed in a handmade 3D-printed cell with the PalmSens4 potentiostat (Netherlands) in a three-electrode cell with pristine- or polyelectrolyte-modified GaP(100) as working electrodes, an Ag/AgCl (KCl sat.) reference electrode, and a Pt wire as a counter electrode. Specimen of GaP was made in contact with the copper plate from the back unpolished side, pressed against it, and fixed to obtain stable ohmic contact. Photocurrent measurements were performed in 1 M KCl or 1 M H_2SO_4 solution under chopped illumination by visible light. Measurements were carried out in two regimes: potential scan from 0.2 to −1.2 V versus Ag/AgCl and chronoamperometry at −0.6 V versus Ag/AgCl. Prior measurement, each specimen was equilibrated in solution at OCP for 5−10 min in the dark.

AUTHOR INFORMATION

Corresponding Author

Ekaterina V. Skorb − *ITMO University, St. Petersburg 191002, Russian Federation;* orcid.org/0000-0003-0888-1693; Email: skorb@itmo.ru

Authors

Nikolay V. Ryzhkov − *ITMO University, St. Petersburg 191002, Russian Federation*

Olesya Ledovich − *ITMO University, St. Petersburg 191002, Russian Federation*

Lara Eggert − *Technical University Ilmenau, Ilmenau 98693, Germany*

Andreas Bund − *Technical University Ilmenau, Ilmenau 98693, Germany;* orcid.org/0000-0001-9837-2408

Agnieszka Paszuk − *Technical University Ilmenau, Ilmenau 98693, Germany*

Thomas Hannappel − *Technical University Ilmenau, Ilmenau 98693, Germany*

Konstantin Klyukin − *Department of Chemical and Biomolecular Engineering, University of Nebraska-Lincoln, Lincoln, Nebraska 68588, United States;* orcid.org/0000-0001-8325-8725

Vitaly Alexandrov − *Department of Chemical and Biomolecular Engineering, University of Nebraska-Lincoln, Lincoln, Nebraska 68588, United States;* orcid.org/0000-0003-2063-6914

Complete contact information is available at: https://pubs.acs.org/10.1021/acsanm.0c02768

Notes

The authors declare no competing financial interest.

https://dx.doi.org/10.1021/acsanm.0c02768
ACS Appl. Nano Mater. 2021, 4, 425−431

■ ACKNOWLEDGMENTS

The reported study was funded by RSF grant no. 19-19-00508. Part of this work was supported by the German Federal Ministry of Education and Research (BMBF proj. no. 033RC021A). A.P. acknowledges the support by the German Research Foundation (DFG), project number PAK 981/3.

■ REFERENCES

(1) Hisatomi, T.; Kubota, J.; Domen, K. Recent Advances in Semiconductors for Photocatalytic and Photoelectrochemical Water Splitting. *Chem. Soc. Rev.* **2014**, *43*, 7520−7535.
(2) Dimroth, F.; Grave, M.; Beutel, P.; Fiedeler, U.; Karcher, C.; Tibbits, T. N. D.; Oliva, E.; Siefer, G.; Schachtner, M.; Wekkeli, A.; Bett, A. W.; Krause, R.; Piccin, M.; Blanc, N.; Drazek, C.; Guiot, E.; Ghyselen, B.; Salvetat, T.; Tauzin, A.; Signamarcheix, T.; Dobrich, A.; Hannappel, T.; Schwarzburg, K. Wafer Bonded Four-Junction GaInP/GaAs//GaInAsP/GaInAs Concentrator Solar Cells with 44.7% Efficiency. *Prog. Photovoltaics Res. Appl.* **2014**, *22*, 277−282.
(3) Cheng, W.-H.; Richter, M. H.; May, M. M.; Ohlmann, J.; Lackner, D.; Dimroth, F.; Hannappel, T.; Atwater, H. A.; Lewerenz, H.-J. Monolithic Photoelectrochemical Device for Direct Water Splitting with 19% Efficiency. *ACS Energy Lett.* **2018**, *3*, 1795−1800.
(4) Standing, A.; Assali, S.; Gao, L.; Verheijen, M. A.; Dam, D. V.; Cui, Y.; Notten, P. H. L.; Haverkort, J. E. M.; Bakkers, E. P. A. M. Efficient Water Reduction with Gallium Phosphide Nanowires. *Nat. Commun.* **2015**, *6*, 7824.
(5) Pishgar, S.; Strain, J. M.; Gulati, S.; Sumanasekera, G.; Gupta, G.; Spurgeon, J. M. Investigation of the Photocorrosion of n-GaP Photoanodes in Acid with in situ UV-Vis Spectroscopy. *J. Mater. Chem. A* **2019**, *7*, 25377−25388.
(6) Butler, M. A.; Ginley, D. S. P-Type GaP as a Semiconducting Photoelectrode. *J. Electrochem. Soc.* **1980**, *127*, 1273.
(7) Tee, S. Y.; Win, K. Y.; Teo, W. S.; Koh, L.-D.; Liu, S.; Teng, C. P.; Han, M.-Y. Recent Progress in Energy-Driven Water Splitting. *Adv. Sci.* **2017**, *4*, 1600337.
(8) Meek, R. L.; Schumaker, N. E. Anodic Dissolution and Selective Etching of Gallium Phosphide. *J. Electrochem. Soc.* **1972**, *119*, 1148.
(9) Madou, M. J.; Cardon, F.; Gomes, W. P. Anodic Processes at the n- and p-Type GaP Electrodes. *Berichte der Bunsengesellschaft für physikalische Chemie* **1977**, *81*, 1186−1190.
(10) Ryzhkov, N. V.; Andreeva, D. V.; Skorb, E. V. Coupling PH-Regulated Multilayers with Inorganic Surfaces for Bionic Devices and Infochemistry. *Langmuir* **2019**, *35*, 8543−8556.
(11) Ryzhkov, N. V.; Brezhneva, N.; Skorb, E. V. Feedback mechanisms at inorganic-polyelectrolyte interfaces for applied materials. *Surf. Innovations* **2019**, *7*, 145−167.
(12) Andreeva, D. V.; Skorb, E. V.; Shchukin, D. G. Layer-by-Layer Polyelectrolyte/Inhibitor Nanostructures for Metal Corrosion Protection. *Appl. Mater. Interfaces* **2010**, *2*, 1954−1962.
(13) Skorb, E. V.; Skirtach, A. G.; Sviridov, D. V.; Shchukin, D. G.; Möhwald, H. Laser-Controllable Coatings for Corrosion Protection. *ACS Nano* **2009**, *3*, 1753−1760.
(14) Andreeva, D. V.; Fix, D.; Möhwald, H.; Shchukin, D. G. Buffering Polyelectrolyte Multilayers for Active Corrosion Protection. *J. Mater. Chem.* **2008**, *18*, 1738.
(15) Brezhneva, N.; Nikitina, A.; Ryzhkov, N.; Klestova, A.; Vinogradov, A. V.; Skorb, E. V. Importance of Buffering Nanolayer Position in Layer-by-Layer Assembly on Titania Based Hybrid Photoactivity. *J. Sol. Gel Sci. Technol.* **2018**, *89*, 92−100.
(16) Tago, T.; Shibata, H.; Nishide, H. Proton Conductivity in the Dry Membrane of Poly(Sulfonic Acid) and Polyamine Layer-by-Layer Complex. *Chem. Commun.* **2007**, 2989.
(17) Fares, H. M.; Schlenoff, J. B. Diffusion of Sites versus Polymers in Polyelectrolyte Complexes and Multilayers. *J. Am. Chem. Soc.* **2017**, *139*, 14656−14667.
(18) Hiller, J. A.; Mendelsohn, J. D.; Rubner, M. F. Reversibly Erasable Nanoporous Anti-Reflection Coatings from Polyelectrolyte Multilayers. *Nat. Mater.* **2002**, *1*, 59−63.
(19) Antipov, A. A.; Sukhorukov, G. B.; Möhwald, H. Influence of the Ionic Strength on the Polyelectrolyte Multilayers' Permeability. *Langmuir* **2003**, *19*, 2444−2448.
(20) Ryzhkov, N. V.; Skorb, E. V. A Platform for Light-Controlled Formation of Free-Stranding Lipid Membranes. *J. R. Soc. Interface* **2020**, *17*, 20190740.
(21) Ulasevich, S.; Ryzhkov, N. V.; Andreeva, D. V.; Özden, D. S.; Piskin, E.; Skorb, E. V. Light-to-Heat Photothermal Dynamic Properties of Polypyrrole-Based Coating for Regenerative Therapy and Lab-on-a-Chip Applications. *Adv. Mater. Interfaces* **2020**, *7*, 2000980.
(22) Jin, J.; Walczak, K.; Singh, M. R.; Karp, C.; Lewis, N. S.; Xiang, C. An Experimental and Modeling/Simulation-Based Evaluation of the Efficiency and Operational Performance Characteristics of an Integrated, Membrane-Free, Neutral PH Solar-Driven Water-Splitting System. *Energy Environ. Sci.* **2014**, *7*, 3371−3380.
(23) Wood, B. C.; Schwegler, E.; Choi, W. I.; Ogitsu, T. Hydrogen-Bond Dynamics of Water at the Interface with InP/GaP(001) and the Implications for Photoelectrochemistry. *J. Am. Chem. Soc.* **2013**, *135*, 15774−15783.
(24) Wood, B. C.; Schwegler, E.; Choi, W. I.; Ogitsu, T. Surface Chemistry of GaP(001) and InP(001) in Contact with Water. *J. Phys. Chem. C* **2014**, *118*, 1062−1070.
(25) Ghosh, S.; Soudackov, A. V.; Hammes-Schiffer, S. Role of Proton Diffusion in the Nonexponential Kinetics of Proton-Coupled Electron Transfer from Photoreduced ZnO Nanocrystals. *ACS Nano* **2017**, *11*, 10295−10302.
(26) Shiratori, S. S.; Rubner, M. F. pH-Dependent Thickness Behavior of Sequentially Adsorbed Layers of Weak Polyelectrolytes. *Macromolecules* **2000**, *33*, 4213−4219.
(27) Curtis, K. A.; Miller, D.; Millard, P.; Basu, S.; Horkay, F.; Chandran, P. L. Unusual Salt and PH Induced Changes in Polyethylenimine Solutions. *PLoS One* **2016**, *11*, No. e0158147.
(28) Ryzhkov, N. V.; Brezhneva, N.; Skorb, E. V. Feedback mechanisms at inorganic-polyelectrolyte interfaces for applied materials. *Surf. Innovations* **2019**, *7*, 145−167.
(29) Skorb, E. V.; Andreeva, D. V. Self-Healing Properties of Layer-by-Layer Assembled Multilayers. *Polym. Int.* **2015**, *64*, 713−723.
(30) Memming, R.; Schwandt, G. Electrochemical Properties of Gallium Phosphide in Aqueous Solutions. *Electrochim. Acta* **1968**, *13*, 1299−1310.
(31) Sekizawa, K.; Oh-Ishi, K.; Morikawa, T. Photoelectrochemical Water-Splitting over a Surface Modified p-Type Cr2O3 Photocathode. *Dalton Trans.* **2020**, *49*, 659−666.
(32) Sprik, M.; Ciccotti, G. Free Energy from Constrained Molecular Dynamics. *J. Chem. Phys.* **1998**, *109*, 7737−7744.
(33) Shi-Gang, S.; Yan, L.; Nan-Hai, L.; Ji-Qian, M. Kinetics of Dissociative Adsorption of Formic-Acid on Pt(100), Pt(610), Pt(210) and Pt(110) Single-Crystal Electrodes in Perchloric-Acid Solutions. *J. Electroanal. Chem.* **1994**, *370*, 273−280.
(34) Perdew, J. P.; Burke, K.; Ernzerhof, M. Generalized Gradient Approximation Made Simple. *Phys. Rev. Lett.* **1996**, *77*, 3865−3868.
(35) Ehrlich, S.; Moellmann, J.; Reckien, W.; Bredow, T.; Grimme, S. System-Dependent Dispersion Coefficients for the DFT-D3 Treatment of Adsorption Processes on Ionic Surfaces. *ChemPhysChem* **2011**, *12*, 3414−3420.
(36) Martyna, G. J.; Klein, M. L.; Tuckerman, M. Nosé-Hoover chains: The canonical ensemble via continuous dynamics. *J. Chem. Phys.* **1992**, *97*, 2635−2643.
(37) Klyukin, K.; Rosso, K. M.; Alexandrov, V. Iron Dissolution from Goethite (α-FeOOH) Surfaces in Water by Ab Initio Enhanced Free-Energy Simulations. *J. Phys. Chem. C* **2018**, *122*, 16086−16091.
(38) Leung, K. First-Principles Modeling of Mn(II) Migration above and Dissolution from LixMn2O4 (001) Surfaces. *Chem. Mater.* **2016**, *29*, 2550−2562.
(39) Xiao, H.; Goddard, W. A.; Cheng, T.; Liu, Y. Cu metal embedded in oxidized matrix catalyst to promote CO 2 activation and CO dimerization for electrochemical reduction of CO 2. *PNAS* **2017**, *114*, 6685.

https://dx.doi.org/10.1021/acsanm.0c02768
ACS Appl. Nano Mater. 2021, 4, 425−431